

UCRL 2417 1
UNCLASSIFIED

UNIVERSITY OF
CALIFORNIA

*Radiation
Laboratory*



BERKELEY, CALIFORNIA

DISCLAIMER

This document was prepared as an account of work sponsored by the United States Government. While this document is believed to contain correct information, neither the United States Government nor any agency thereof, nor the Regents of the University of California, nor any of their employees, makes any warranty, express or implied, or assumes any legal responsibility for the accuracy, completeness, or usefulness of any information, apparatus, product, or process disclosed, or represents that its use would not infringe privately owned rights. Reference herein to any specific commercial product, process, or service by its trade name, trademark, manufacturer, or otherwise, does not necessarily constitute or imply its endorsement, recommendation, or favoring by the United States Government or any agency thereof, or the Regents of the University of California. The views and opinions of authors expressed herein do not necessarily state or reflect those of the United States Government or any agency thereof or the Regents of the University of California.

UNIVERSITY OF CALIFORNIA

Radiation Laboratory

Contract No. W-7405-eng-48

EXCITATION FUNCTION FOR POSITIVE PIONS PRODUCED
AT 90° IN PROTON-CARBON COLLISIONS

Daniel Allen Hamlin

(Thesis)

November 20, 1953

Berkeley, California

EXCITATION FUNCTION FOR POSITIVE PIONS PRODUCED
AT 90° IN PROTON-CARBON COLLISIONS

Table of Contents

| | <u>Page</u> |
|--|-------------|
| ABSTRACT | 4 |
| I. INTRODUCTION | 5 |
| II. APPARATUS AND PROCEDURE | 6 |
| A. General Description of the Experiment | 6 |
| B. Experimental Details | 6 |
| 1. Proton Source and Collimation | 6 |
| 2. Beam Monitor | 8 |
| 3. Proton Energy Degradation | 8 |
| 4. Target | 9 |
| 5. Magnet and Channel | 9 |
| 6. Pion Energy Degradation | 10 |
| 7. Scintillation Counter Telescope | 10 |
| C. Pion Identification | 11 |
| 1. Introduction | 11 |
| 2. General Method | 11 |
| 3. Detection Validity | 17 |
| III. ANALYSIS OF DATA | 20 |
| A. Detection Efficiency Normalization | 20 |
| B. Corrections | 22 |
| 1. Nuclear Interaction of Protons | 23 |
| 2. Thick Target | 24 |
| 3. Energy Dependence of Detection Interval | 25 |
| 4. Pion Decay in Flight | 25 |
| 5. Nuclear Interaction of Pions | 25 |
| 6. Solid Angle | 26 |
| 7. Muon Decay | 26 |
| 8. Summary | 27 |
| C. Integration of Spectra | 28 |
| D. Normalization for Absolute Values | 28 |
| IV. RESULTS | 30 |

| | <u>Page</u> |
|---|-------------|
| V. DISCUSSION | 34 |
| VI. ACKNOWLEDGMENTS | 38 |
| VII. APPENDICES | 39 |
| A. Smoothing of Background Fluctuations | 39 |
| B. Description of Electronics | 39 |
| C. Voltages, Plateaus, and Detection Efficiencies | 44 |
| D. Detection Efficiency Normalization Formula | 47 |
| E. Thick-Target Correction Factor | 48 |
| F. Multiple Coulomb Scattering | 50 |
| 1. Distribution Functions | 50 |
| 2. Loss Due to an Aperture | 51 |
| REFERENCES | 54 |

EXCITATION FUNCTION FOR POSITIVE PIONS PRODUCED
AT 90° IN PROTON-CARBON COLLISIONS

Daniel Allen Hamlin

Radiation Laboratory, Department of Physics
University of California, Berkeley, California

November 20, 1953

ABSTRACT

The differential cross section for positive pions produced at 90° in the reaction $p + C \rightarrow \pi^+$ was measured in the proton energy interval 235 to 336 Mev. Pions emitted at 90° from the target bombarded by the external proton beam of the Berkeley 184-inch synchrocyclotron were identified by the use of a scintillation counter telescope and delayed coincidence based on the $\pi^+ - \mu^+$ decay. The pion energy spectrum obtained at each proton energy was corrected and integrated to obtain the relative yields that are shown below (together with standard deviations due to statistics of counting).

Relative Yield at 90° for $p + C \rightarrow \pi^+$

| T_{proton} (Mev) | 235 | 264 | 294 | 313 | 336 |
|--|-------------------|-------------------|-------------------|-------------------|--------------------|
| Relative $\frac{d\sigma(T_p, 90^\circ)}{d\Omega_{\text{lab}}}$ | 14.7 ± 2.4 | 30.5 ± 3.4 | 43.9 ± 4.3 | 76.6 ± 3.0 | 100.0 ± 3.6 |

For the assumed power law $d\sigma/d\Omega \sim (T_p - T_0)^b$ the exponent (calculated by least squares) is 2.5 ± 0.6 ; T_0 was taken to be the absolute threshold (~ 150 Mev) for this reaction. Normalization to nuclear emulsion data sets the absolute scale at $T_p = 336$ Mev to be $d\sigma(336, 90^\circ)/d\Omega_{\text{lab}} = (3.20 \pm 0.16) \times 10^{-28} \text{ cm}^2/\text{sterad}$.

EXCITATION FUNCTION FOR POSITIVE PIONS PRODUCED
AT 90° IN PROTON-CARBON COLLISIONS

Daniel Allen Hamlin

Radiation Laboratory, Department of Physics
University of California, Berkeley, California

November 20, 1953

I. INTRODUCTION

The production of charged pions from carbon bombarded by high-energy protons has been studied by numerous workers. The first measurement was made by Jones and White,¹ who determined the relative yield of negative pions (2 to 10 Mev and 0 to 45° to the beam) for the proton energy interval 165 to 345 Mev. For 340-Mev protons there have been measurements of the complete energy spectra for both positive and negative pions produced at various angles to the beam: at 90° by Richman and Wilcox² and later by Dudziak³, at 0° by Dudziak⁴, and at 180° by Leonard.⁵ Passman et al.⁶ have obtained pion energy spectra at 90° for proton energies 345, 365, and 380 Mev.

The completion of the picture of charged-pion production from carbon (and hence from any complex nucleus to the extent that carbon is typical) was regarded as worth while. Consequently, the experiment described here was undertaken to measure the positive-pion excitation function for an appreciable proton energy interval extending downward from 340 Mev. The angle of 90° was selected owing to the above-mentioned data at higher proton energies and to experimental feasibility.

A general description of the experiment and the equipment used is given in the next section. In Section III the treatment of the raw data and corrections are described. The final results are presented and discussed in Sections IV and V.

II. APPARATUS AND PROCEDURE

A. General Description of the Experiment

The general method employed in this experiment is similar to that used by Schulz.⁷ A 340-Mev proton beam, after traversing an ionization chamber whose integrated current served as the beam monitor, passed through an amount of energy degrader appropriate for obtaining an energy down to 240 Mev. As shown in Fig. 1 the beam then struck a carbon target placed near the degrader and inside a magnetic field. Positive pions emitted from the target at $90^\circ \pm 3.3^\circ$ to the beam were turned through approximately 90° by the magnetic field while passing between the walls of a channel. Upon leaving the channel at the edge of the pole faces, the pion passed through a copper degrader of such thickness that the pion to be detected stopped in the last crystal of a three-crystal scintillation counter telescope. The pion's passage through the first and second crystals initiated a delayed signal which was put in coincidence with the muon pulse arising from the pion's decay. At each proton energy the pion energy spectrum was scanned above the 21-Mev threshold of the counter telescope. The integrals of the histograms determined by the corrected data gave the relative differential cross sections per unit solid angle for positive pions at 90° in the reaction $p + C \rightarrow \pi^+$.

B. Experimental Details

1. Proton Source and Collimation. The source of the protons was the external scattered proton beam from the Berkeley 184-inch synchrocyclotron. Some facts useful for counter work are that during each fm pulse (which has a repetition rate of about 55/sec.) the beam comes out in roughly 300 short ($\sim 0.5 \times 10^{-8}$ sec.) rf bursts which are separated by 6.0×10^{-8} sec.

The mechanism for production of the scattered⁸ beam is, in principle, that a portion of the full-energy circulating proton beam that traverses a thin scatterer placed in its path is multiply scattered at such an angle that it passes into the magnetic deflecting channel. Upon leaving the main vacuum chamber, as shown in Fig. 1, the protons enter an evacuated tube through which they travel while they are collimated--once in front of the focusing magnet, and again by a 48-inch-long brass collimator jutting

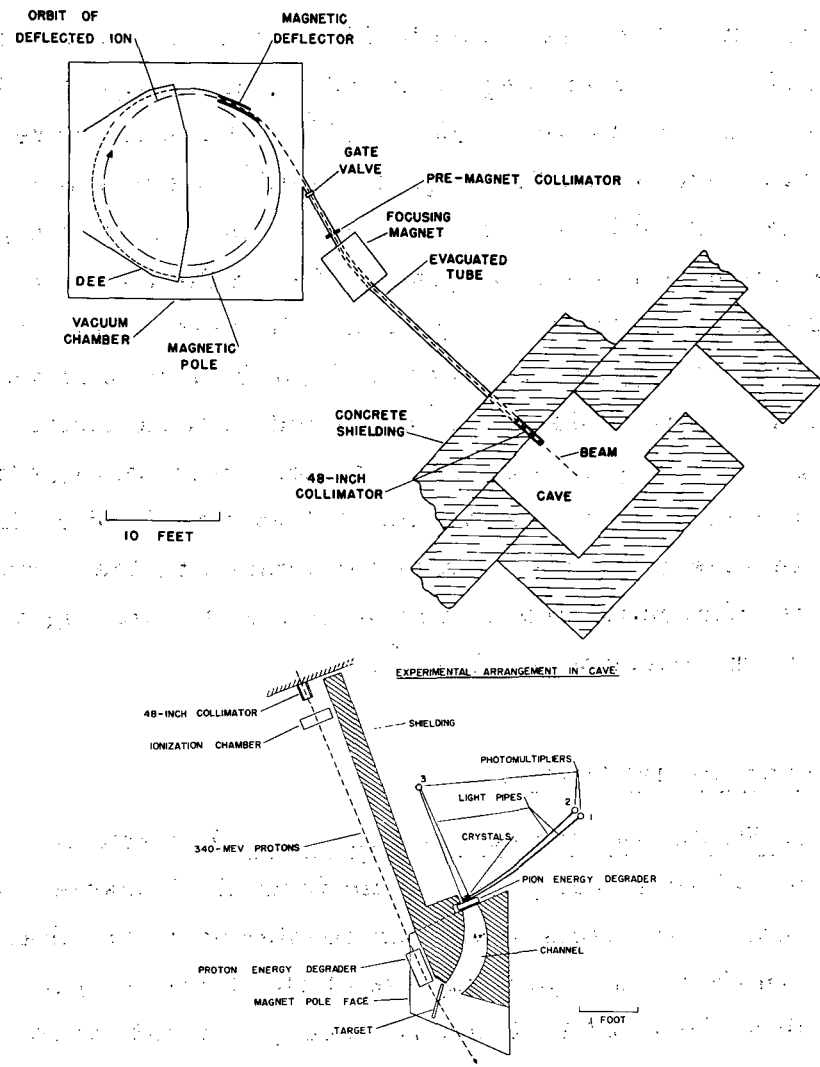


Fig. 1 - Schematic diagram of cyclotron and cave showing the trajectory of the external proton beam. The experimental arrangement in the cave is shown in the lower figure.

out of the main concrete shielding into an annex known as the 'cave' in which experiments may be performed.

The amount of background in the cave may be reduced somewhat by minimizing the beam's scraping of the 48-inch collimator. This minimization is made possible by the facts that, for appropriate settings of the collimator preceding the focusing magnet, the scattered beam tends to be concentrated in an approximately horizontal line⁹ and the beam may be laterally confined to a width narrower than that of the 48-inch collimator used. In this experiment the horizontal and vertical dimensions of the premagnet and 48-inch collimators were, respectively, 0.30 in. x 0.20 in. and 1.25 in. x 0.75 in. The beam entering the cave was essentially contained within a rectangle 0.6 in. x 0.75 in.

2. Beam Monitor. The beam-monitoring apparatus (standard equipment at University of California Radiation Laboratory) consisted basically of an ionization chamber that produced a charge proportional to the number of traversing protons, an integrating electrometer that summed the charges from the ionization chamber, and a recorder that continuously indicated a voltage proportional to the charge collected.

The multiplication factor of the ionization chamber (similar to that described in reference 10) was assumed to remain constant during the course of a given run; its value, however, did not have to be known or to be the same on different runs since, as is discussed later, the pion-detection efficiency of the counter system had to be normalized from run to run.

3. Proton Energy Degradation. The merits of degrading the beam's energy immediately in front of the target were that the beam was easily monitored in an accurate manner, that the usable beam intensity was not significantly decreased by the beam's divergence caused by the multiple Coulomb scattering in the degrader, and that the necessarily frequent changes in the amount of degrader were made quickly.

Carbon was selected from the low-atomic-number elements for the degrader material simply because it adequately reduced the multiple scattering for the geometry employed and was readily available in the quantity needed. Aron's range-energy tables¹¹ were used for determining the amounts of degrader required for the desired energies. The surface densities were calculated from the measurements for each of the 15

accurately milled and weighed pieces obtained from a single slab of one-half inch thickness. In passing through the 7.5 in. of carbon used for degrading from 340 to 240 Mev, the beam increased in the lateral dimension from 1.0 to 1.5 in.

4. Target. A target as thick as was compatible with keeping the thick-target corrections from becoming unduly large was necessitated by the low counting rates--from 3.8 to 0.1 counts/min. A compromise was reached by using one target of 1.46 gm/cm^2 in the beam direction for the lower two pion energies and another of twice that thickness for the higher energies. The target, aligned with its plane at 45° to the beam as shown in Fig. 1, presented an area considerably larger than that of the beam for all proton energies used.

5. Magnet and Channel. The utility of the channel in conjunction with the magnetic field was that the number of background particles was greatly reduced by preventing high-energy protons from passing from the target to the detector. This separation was possible because the ratio of the ranges of protons and pions of the same momentum is much less than unity.

The requirements imposed on the design of the channel were that all the pions in the energy interval accepted by the telescope be able to pass from any point of the target struck by the proton beam to any point of the detector, that the exit size of the channel be relatively large compared to the detector in order that corrections be small for multiple Coulomb scattering in the copper pion degrader, and that all the pion orbits be kept in a field as uniform as possible. These requirements were met by the use of two channels (having central radii of curvature of 16 and 22 in.), whereby the energy intervals 20 to 80 Mev and 60 to 120 Mev could be scanned. As a direct experimental check that the orbits of the pions to be accepted by the telescope were contained well within the confines of the channels and also passed through the fringing field near the channel exit as predicted, the orbits for pions of various energies were simulated by a stretched wire carrying a current $i = 10t/Hp$ (i in amps., t in dynes, Hp in gauss-cm), where Hp is related to the pion's momentum by $eHp = cp$ for a uniform magnetic field.

The source of the magnetic field was an electromagnet (originally designed as an electron-pair spectrometer) that could produce a maximum field of about 14.3 kilogauss in a 3.4-in. gap. The magnetization curve and field uniformity were determined by a proton magnetic resonance apparatus. Secured to the lower pole face of the magnet was a brass base plate on which the position of the internal assembly could be accurately reproduced from run to run by means of studs and holes. The exposure of two fiducially marked x-ray films to the proton beam facilitated the alignment of the magnet with respect to the beam.

6. Pion Energy Degradation. Degraders placed at the channel's exit and immediately in front of the crystals allowed pions of different energies to be accepted by the counter telescope. Copper was used as the degrader material because it possesses both compactness and tolerable multiple-scattering effects. The transverse dimensions of the copper slabs were larger than the exit size of the channel; hence, the multiple-scattering corrections for pions depended only on the channel and crystal sizes and the thickness of the copper.

7. Scintillation Counter Telescope. The scintillation counter telescope was comprised basically of a set of three crystals, each viewed by a photomultiplier tube that gave an output pulse when the crystal scintillated owing to the passage of a charged particle. Because the operation of the photomultipliers would have been adversely affected by the strong magnetic field existing in the region in which the crystals were necessarily located, lucite light pipes were used to transmit the scintillations from the crystals to the photomultipliers located about two feet from the edge of the gap. See Fig. 1.

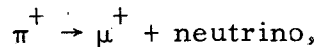
The extremely clear trans-stilbene crystals, grown by Drs. Calvin André and James Carothers, were approximately two inches square and about 0.9, 0.6, and 1.0 gm/cm² in thickness. A pion having an energy of 18.3 Mev (or 23.8 Mev), upon entering the telescope, stopped at the front (or back) of the third crystal. The range of a 4.1-Mev muon in trans-stilbene is 0.14 gm/cm². (The range-energy relation used for trans-stilbene was one obtained on the usual assumption that the stopping power of a material is the sum of the stopping powers of its constituents.¹²)

The photomultipliers were RCA 1P21's. No attempt was made to clip the pulses. The tubes were mounted within a 1/16-in. steel housing which was inclosed in 1/4-in. steel. That this mounting was adequate for magnetic shielding was tested by use of a γ -ray source. For a change of 7000 gauss in the gap, as occurred in the experiment, the output pulse height changed by less than two percent.

C. Pion Identification

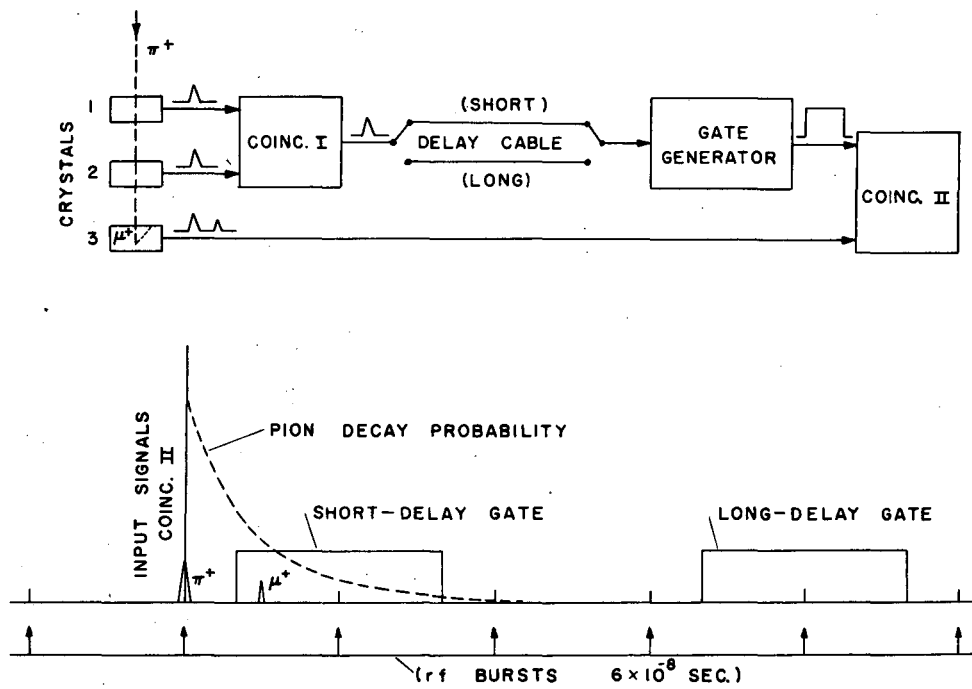
1. Introduction. The historical development of the electronics for the identification of positive pions is briefly as follows: Mesons have been detected by previous investigators¹³ using coincidence techniques based on the $\mu^+ \rightarrow \beta^+$ decay. A detection system, similar to those of the early workers but based on the nearly one hundred times faster $\pi^+ \rightarrow \mu^+$ decay, was designed by Jakobson¹⁴ and used in various experiments¹⁴⁻¹⁶ for detecting positive pions. The incorporation of two refinements into Jakobson's original system produced the one used in this and other experiments,^{7, 17} and which is now described.

2. General Method. The identification of the pions was based on the fact that a positive pion characteristically decays into a positive muon in accordance with the scheme¹⁸



for which the mean life¹⁴ of the spontaneous decay is 2.54×10^{-8} sec. and the energy¹⁹ of the muon is 4.1 Mev. This decay was utilized in the requirement of a coincidence of the muon signal and an appropriately delayed signal from the pion.

The essential method by which the signals from the scintillation counter telescope were mixed to provide identification of the pions can be understood with the aid of Fig. 2, which is a simplified block diagram of the basic electronics and method. According to this diagram the two signals ($\sim 10^{-8}$ sec. duration) from photomultipliers Nos. 1 and 2, resulting from the passage of a charged particle through crystals Nos. 1 and 2, were sent through equal lengths of coaxial cable to coincidence circuit I (CI). The output pulse ($\sim 10^{-8}$ sec.) from CI was sent through a selected length of delay cable to a gate generator (GG) whose output, a rectangular voltage pulse ($\sim 10^{-7}$ sec.), was sent to CII. If the given charged particle



SIMPLIFIED DIAGRAM OF ELECTRONICS AND METHOD

Fig. 2 - Simplified diagram illustrating the method of positive pion production.

was a positive pion and if, further, it stopped in crystal No. 3, then both the pion's entry signal and the subsequent muon decay signal were also sent to CII. The relative lengths of cable involved were so chosen that if the output of CI was sent through the short-delay cable, then the gate signal arrived at CII a little after the pion's entry signal.* If the gate's delay relative to the pion's entry signal was approximately equal to the pion's mean life, then for about 37 percent of the pions stopping in the third crystal there was simultaneity of the muon and gate signals, since the gate's length was long compared to the pion's mean life. For those cases of simultaneity CII gave a resultant output that was registered and counted as a positive pion.

It is evident that there could have been in the crystals a sequence of pulses of nonpionic origin that would cause the electronics to register as a pion. For example, a nonpionic charged particle (or a pion with either too little or too much energy to stop in the third crystal) produced during a given rf burst could have caused a gate to be generated; and another charged particle produced during the next rf burst could have passed through the third crystal. This accidental type of event, or background, had to be measured and subtracted from the total number of counts obtained with the short-delay cable in order to get the net or true pion counts.

It was assumed that the background pulses in the third crystal were random, at least to the extent that the beam intensity did not change appreciably over a period of approximately one-half dozen rf bursts. Consequently, the background was measured by causing the gate to be delayed a time equal to many (about eight) mean lifetimes of the pion, as shown in Fig. 2. The only restrictions were that this long delay be small (about one percent in this experiment) compared to the length of a fm pulse and that the same number of rf bursts occur during the long-delayed gate as during the short-delayed gate.

* The selection of a safe minimum length for the short-delay cable was checked by making a mean-life measurement. It is easily seen that if one had not delayed the gate a sufficient amount, then the signal resulting from simply the pion's (or even a nonpionic charged particle's) entry into the third crystal would have fallen into the gate.

In actual practice the pions and background particles were measured essentially simultaneously by using, in principle, two identical GG's and two identical CII's. In this arrangement, as shown in Fig. 3, the output of CI was split so that its signal traveled down both a short- and a long-delay cable and fed into GG-A and GG-B, respectively. The output of the third photomultiplier was likewise split so that its output signal traveled down two cables and fed into CII-A and CII-B. Thus, both short- and long-delayed gates were generated each time a charged particle passed through the first two crystals. The difference between CII-A's counting rate and that of CII-B was the true pion counting rate.

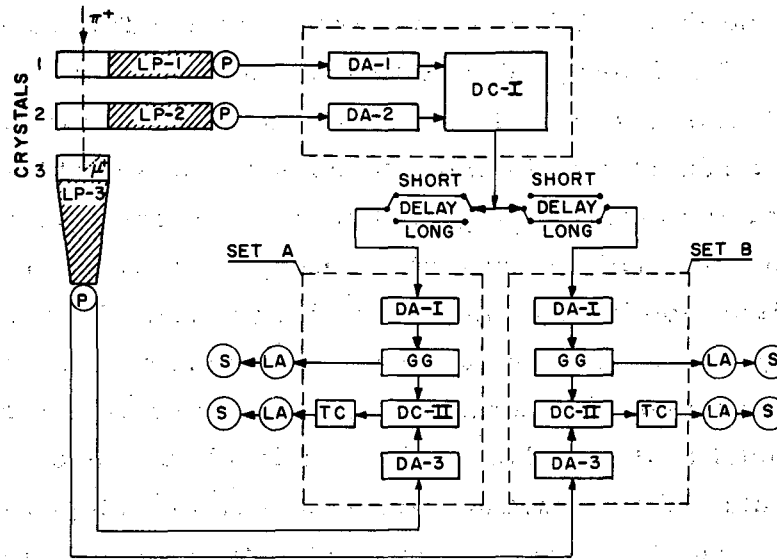
The inherent difficulties in making two sets of electronic equipment with identical characteristics (and hence the same detection efficiencies) were circumvented by interchanging the delay cables for the two sets on successive units of integrated beam. Failure to interchange would have led to systematic errors since one would have been constantly subtracting off either too little or too much background. The end result of this interchange procedure, as discussed in Appendix A, is that the fractional error in the number of true pion counts for two units of integrated beam is proportional to the product of the fractional difference in efficiencies of the two sets and the fractional difference in the integration times.

The two very important advantages that resulted from the use of two sets of delayed-coincidence circuits instead of just one set were that (1) errors due to beam intensity fluctuations were made negligible and (2) cyclotron running time required for an experiment was cut in half.

A description of the electronics is given in Appendix B. Appendix C describes the selection of operating voltages for the photomultipliers. Briefly, the operating voltages for the photomultipliers Nos. 1 and 2 were selected from plateau curves (shown in Fig. 4) and that for No. 3 was selected by another method, since no satisfactory plateau region was found for the positive-pion detection efficiency.

The ratio of pion to background counts ranged from about 4.5, at $T_p = 336$ Mev and $T_\pi = 42.6$ Mev, to about 1.0, at $T_p = 235$ Mev and $T_\pi = 42.6$ Mev. The relative beam intensities in the two cases were six and one.

BLOCK DIAGRAM OF ELECTRONICS



- DA DISTRIBUTED AMPLIFIER
- DC DISTRIBUTED COINCIDENCE
- GG GATE GENERATOR
- LA LINEAR AMPLIFIER
- LP LIGHT PIPE
- P PHOTOMULTIPLIER
- S SCALAR
- TC TRIGGER CIRCUIT

100-6776

Fig. 3 - Complete block diagram of the $\pi^+ - \mu^+$ electronic detection equipment.

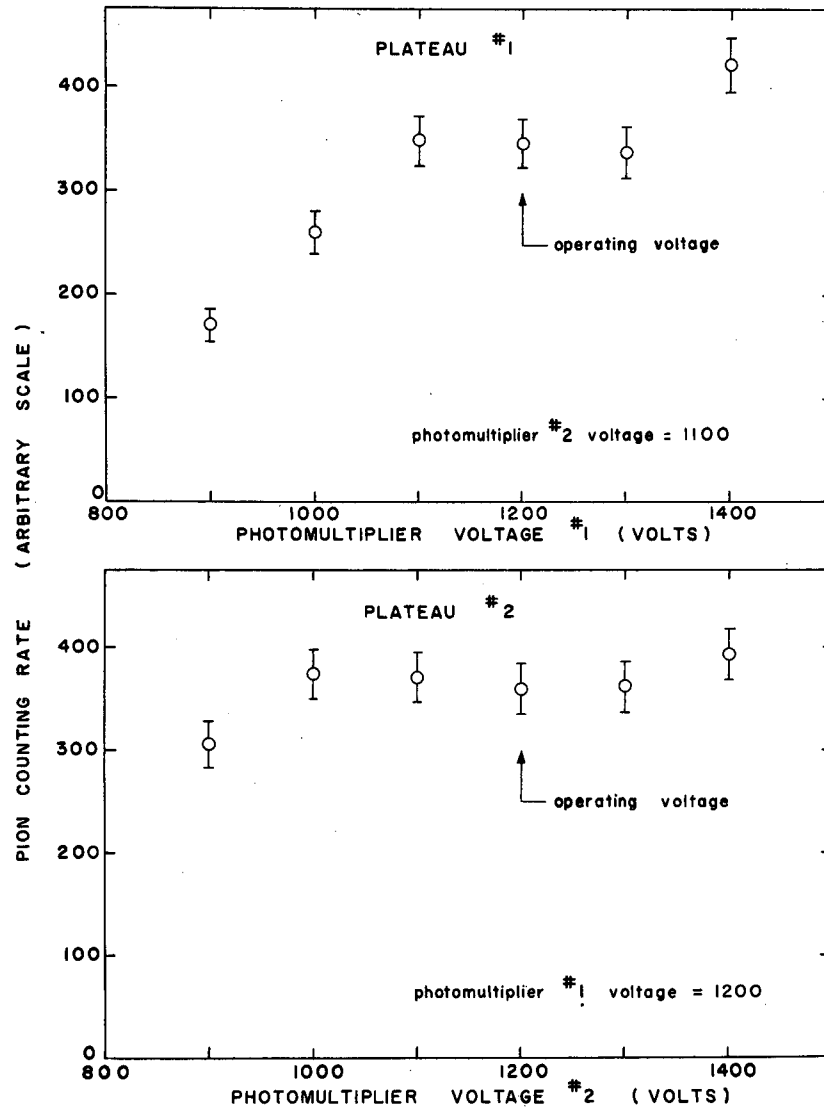


Fig. 4 - Pion counting rate versus voltage applied to photomultiplier No. 1 (upper graph) and photomultiplier No. 2 (lower graph). The operating voltages are indicated.

3. Detection Validity. Evidence is now given that the detection equipment described in this paper actually identified positive pions and distinguished them from other particles. This evidence may be arbitrarily grouped into two categories:

- a) Attempts to reproduce positive-pion characteristics and spectra obtained by other workers and methods.
- b) Attempts to detect positive pions under conditions such that pions were known not to be present.

In the former category the following experiments may be listed:

- 1) The positive-pion mean life was measured on two occasions under very different background conditions (synchrotron and synchrocyclotron). The values obtained^{14,*} are in excellent agreement with that obtained by Wiegand.²⁰
- 2) The shape of the sharply peaked pion spectrum resulting from the reaction $p + p \rightarrow \pi^+ + d$, first measured by Cartwright et al.²¹ using nuclear emulsions, was reproduced by Schulz et al.⁷ using the presently described $\pi^+ - \mu^+$ delayed-coincidence technique. A further comparison is possible since both groups of workers used the polyethylene-carbon subtraction method. The efficiency factor required for normalizing the hydrogen data obtained by the two methods was, within the statistics of the two experiments, the same as that which would be required for normalizing the carbon data.
- 3) At the Berkeley synchrotron positive pions from several gasses were detected¹⁶ by both emulsion techniques and the $\pi^+ - \mu^+$ delayed-coincidence method. The shapes of the spectra obtained by the two methods were in agreement; further, the normalization factors required to normalize the counter data to the emulsion data for the various gasses were the same.
- 4) The shape of the spectrum obtained in this experiment for 336-Mev protons is in agreement with those obtained by several groups

*

The other measurement is discussed in Appendix C-2.

of workers^{2, 3, 6,*} using nuclear emulsion techniques.

In the second category the following tests may be listed:

1) In this experiment the energy of the proton beam was degraded below the absolute threshold^{**} (~ 150 Mev) for positive-pion production from carbon; no net counts were obtained.

2) In the above-mentioned experiment at the synchrotron the photon-beam energy was lowered below the absolute threshold for pion production; again no net counts were obtained.

3) In Merritt's experiment mentioned above, no pions of energy greater than the kinematical maximum for the reaction $p + d \rightarrow \pi^+ + t$ were detected.

* The positive-pion spectrum at 90° for $p + C \rightarrow \pi^+$, obtained by Walter Dudziak using nuclear emulsions, is shown in Fig. 5 with corresponding data obtained in the presently described experiment. The two spectra have been normalized to the same area. The author wishes to express his appreciation to Mr. Dudziak for the use of his experimental data prior to publication.

** The absolute threshold²² energy for the reaction $p + C^{12} \rightarrow \pi^+$ is obtained by applying the conservation theorems and assuming that the entire carbon nucleus (as a unit) is involved in the collision with the incident proton; the end products are assumed to be $C^{13} + \pi^+$.

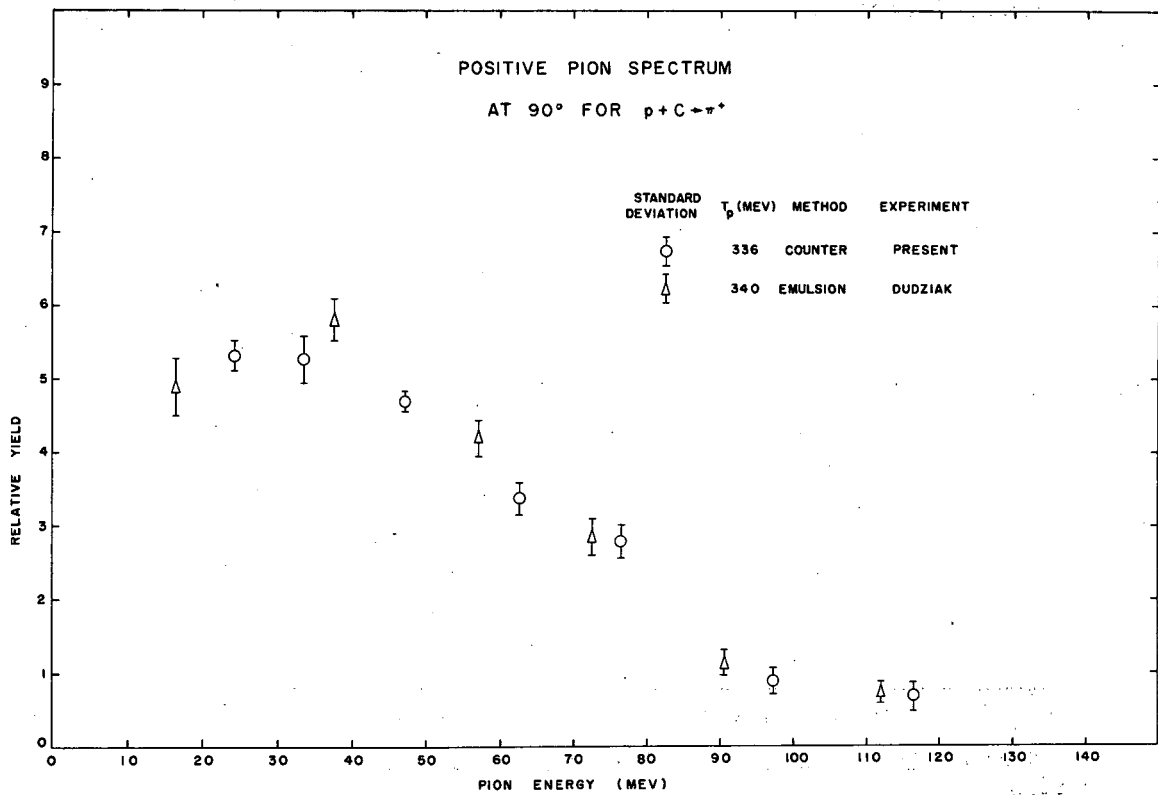


Fig. 5 - Comparison of the present data and those obtained by W. Dudziak for the positive pion spectrum at 90° for $p + C \rightarrow \pi^+$. The two spectra have been normalized to the same area.

III. ANALYSIS OF DATA

A. Detection Efficiency Normalization

The detection efficiency for positive pions varied from run to run (six runs in five months) owing to the lack of a pion counting plateau, as mentioned in Section II-C-2. The basis for circumventing this difficulty lay in the assumption that on different runs the detection equipment would reproduce a given spectrum except for a constant normalization factor k and the statistical fluctuations in counts. The validity of this assumption could be judged from a test for consistency after actually carrying out a suitable normalization of detection efficiencies.

The normalization scheme described in Appendix D is one which utilized as many as possible of the counts obtained during a run. After the k for a pair of runs had been calculated, one then combined them on the basis of internal consistency while propagating the uncertainty due to the normalization. This procedure was then repeated for a third run and the initial two, for a fourth run and the initial three, etc. It can be shown that the final result is independent of the grouping of the runs.

The consistency of the runs was first judged qualitatively and later, quantitatively. After normalizing the detection efficiencies, one calculated at each of the pion energies for 336-Mev protons both the relative number of counts obtained during each of the runs and the weighted mean value, assuming internal consistency for the runs as a group. The weight assigned to each of the relative numbers was taken proportional to the inverse square of its standard deviation. The results of this qualitative test are shown in Fig. 6.

The quantitative test for consistency of the runs is described by Birge.²³ Application of the test at a given pion energy requires one to take the ratio of the standard deviations of the weighted mean value as calculated on the bases of external consistency [$\sigma(\text{ext})$] and internal consistency [$\sigma(\text{int})$]. If the runs are consistent the ratio should equal unity except for the statistical fluctuations arising from the small number of runs.

For each pion energy in Table I ($T_p = 336$ Mev) one find tabulated the number of runs during which data were obtained at that energy; the above discussed ratio, r ; and the ratio's theoretical standard deviation

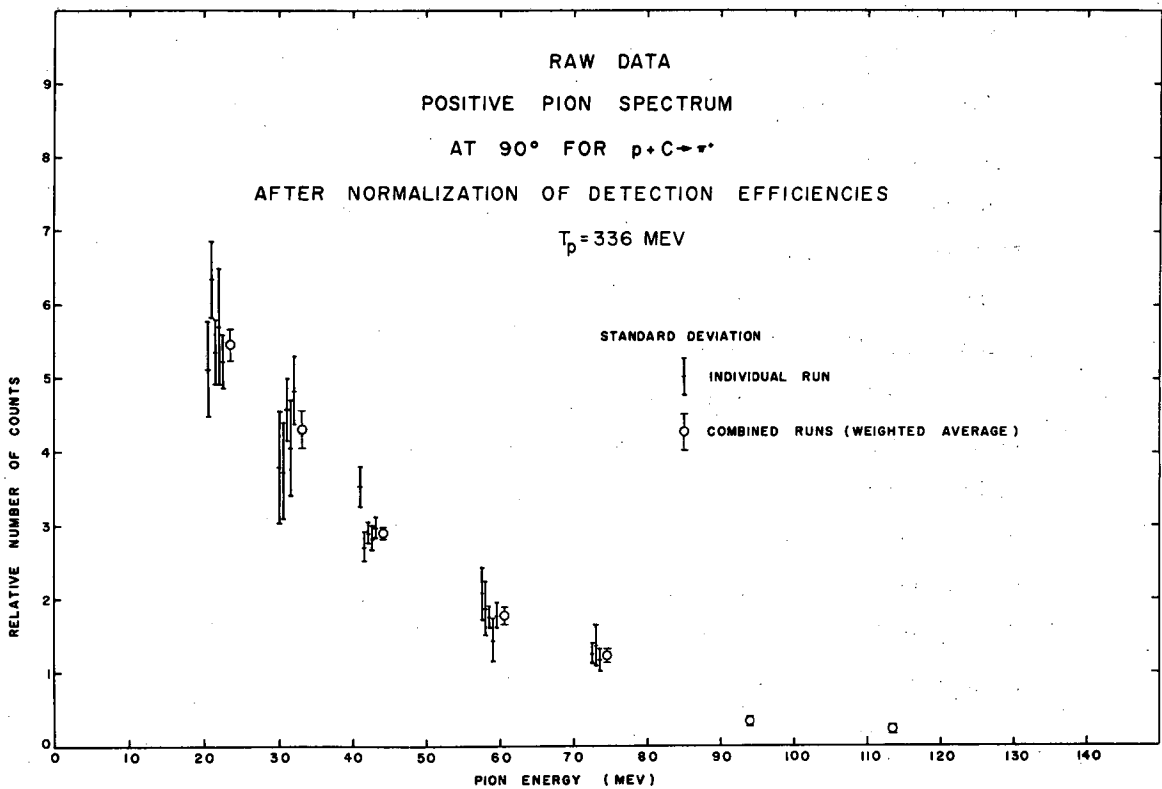


Fig. 6 - A graph showing the reproducibility obtained (after normalization of detection efficiencies) from the $\pi^+ - \mu^+$ electronic detection equipment. Shown are the relative number of pion counts (for $T_p = 336$ Mev) obtained during each of the runs and the weighted average for the runs as a group, assumed to be internally consistent. (The counts are raw data except for solid angle and target-thickness normalizations.)

from unity that corresponds to the number of runs involved, σ_r .

Table I
External-Internal Consistency Test
for Detection Efficiency

| T_π (Mev) | No. of Runs | $\frac{\sigma(\text{ext})}{\sigma(\text{int})} = r$ | σ_r |
|---------------|----------------|---|------------|
| | | | |
| 21.0 | 6 | 0.92 | 0.32 |
| 30.8 | 5 | 0.86 | .35 |
| 42.6 | 5 | 1.27 | .35 |
| 58.8 | 5 | 0.72 | .35 |
| 73.1 | 3 | 0.44 | 0.50 |

One notes that the deviations of r from unity are in satisfactory agreement with the fluctuations expected on statistical grounds. Further, that $|1-r|$ is less than σ_r for four of the five pion energies compares satisfactorily with the a priori expectation that it should be so for 68 percent of the cases.

The conclusion drawn from the above analysis was that the procedure used for normalizing the detection efficiencies was probably valid, together with the assumption on which it was based, namely, that on different runs the detection equipment would statistically reproduce a given spectrum except for a constant normalization factor.

B. Corrections

Listed below are the effects that were examined for their relevancy in applying corrections to the data obtained after normalization of the detection efficiencies:

1. Nuclear interaction of protons in energy degrader
2. Thick target
3. Energy dependence of detection interval

4. Pion decay in flight
5. Nuclear interaction of pions
6. Solid angle
7. Muon decay

1. Nuclear Interaction of Protons. In passing through the energy degrader the incident protons could undergo nuclear interaction which was either inelastic (nuclear absorption) or elastic (nuclear diffraction and multiple Coulomb scattering).

a. Nuclear Absorption. The fractional number of incident protons that did not suffer nuclear absorption in the traversal of n nuclei per cm^2 was $\exp(-n\sigma_{ab})$, where σ_{ab} is the nuclear absorption cross section for carbon. The values used for σ_{ab} are given by the relation

$$\sigma_{ab}(\text{barns}) = 0.240 - 1.72 \times 10^{-4} T_p (\text{Mev}),$$

which is the linear function fitted by least squares to the data of Kirschbaum.²⁴ At each bombardment energy the value of $n\sigma_{ab}$ was obtained by summing $\Delta n\sigma_{ab}(T_p)$ over the degrader and one-half the target thickness. The correction factor for nuclear absorption of protons, $\exp(n\sigma_{ab})$, applied at each of the proton energies, varied from 1.01 at 336 Mev to 1.36 at 235 Mev.

b. Nuclear Diffraction. The fractional number of incident protons that did not suffer a nuclear diffraction scatter through an angle $\theta \geq \theta_0$ in the traversal of n degrader nuclei per cm^2 was $\exp[-n\sigma_d(>\theta_0)]$, where σ_d , the nuclear diffraction cross section for the event considered, is given by

$$\sigma_d(\geq\theta_0) = \int_{\theta_0}^{\pi} (d\sigma_d / d\Omega) 2\pi \sin \theta d\theta.$$

The values used for $d\sigma_d / d\Omega$, the nuclear diffraction cross section per unit solid angle, were, for $T_p = 336$ Mev, those measured by Richardson,⁹ and for $336 \text{ Mev} > T_p \geq 235$ Mev, those obtained from Richardson's values by multiplying the angles by the ratio of de Broglie wave lengths corresponding to the proton energies involved. At each bombardment energy one obtained the value of $n\sigma_d(\geq\theta_0)$ by summing $\Delta n\sigma_d(\geq\theta_0)$ over the degrader while taking into account the dependence of θ_0 on the depth of penetration in the degrader. The nuclear diffraction scattering correction factor, $\exp[n\sigma_d(\geq\theta_0)]$,

applied at each of the proton energies, varied from 1.00 at 336 Mev to 1.03 at 235 Mev.

c. Multiple Coulomb Scattering. The proton beam's lateral and angular displacement due to multiple Coulomb scattering in the energy degrader was calculated from the distribution function derived by Eyges.²⁵ A summary of the formulae is given in Appendix F. As implied earlier, the channel width was so selected that a negligible portion of the proton beam would acquire a lateral displacement outside the usable target bounds as viewed from the channel. Verification of the beam's confinement to such a region was obtained from the previously mentioned x-ray film used for alignment. Hence, no correction was applied.

2. Thick Target. The target's finite thickness gave rise to five effects, for each of which a correction was made.

a) The energy of the proton beam was 2.2 to 5.5 Mev lower at the center of the target than it was at the front surface. The final data are given as a function of the mean bombardment energy.

b) The mean bombarding proton beam energy was 2.2 to 2.7 Mev higher at the two lowest pion-detection energies than at the higher pion energies because targets of different thicknesses were used in the two cases. The effect of the excitation function was taken into account by fitting empirical equations of the form $a(T_p - T_o)^b$ (where a , b , and T_o are constants and T_p is the proton energy) to the data (corrected for nuclear interaction of protons) at the two lowest pion energies. These empirical curves were used for the small interpolations and extrapolations necessary so that the mean bombarding proton energy would be constant for a given pion spectrum. To normalize the yields from the two targets the yield from the thinner target was multiplied by the appropriate ratio of target thicknesses in gm/cm^2 .

c) The nuclear absorption of the proton beam in the target was taken into account in the correction discussed in Section III-B-1.

d) The mean energy of the energy interval for pion production in the target was 3.3 to 4.5 Mev higher than the mean energy of the corresponding interval for pion detection at the front face of the copper degraders. The final data are given as a function of the mean energy for pion production.

e) The average energy interval for pion production in the target, $\overline{(\Delta T)_{\pi x}}$, was less than its corresponding energy interval for pion detection

at the front face of the copper degraders, $(\Delta T_\pi)_d$. The appropriate correction factor, $(\Delta T_\pi)_d / (\overline{\Delta T_\pi})_x$, is derived in Appendix E.

3. Energy Dependence of Detection Interval. The energy dependence of the energy interval for pion detection resulted from the dependence of the quantity $(\Delta T_\pi)_d$ on the amount of degrader placed in front of the telescope. This effect was taken into account by the correction factor $(\Delta T_\pi)_{fl} / (\Delta T_\pi)_d$, where $(\Delta T_\pi)_{fl}$ is the energy interval for pion detection at the front face of the first crystal.

Elimination of the quantity $(\Delta T_\pi)_d$ by multiplication of the correction factors for thick target and energy dependence of the energy interval for pion detection yields $(\Delta T_\pi)_{fl} / (\overline{\Delta T_\pi})_x$, a factor which varied from 1.26 at 21.0 Mev to 2.44 at 113.5 Mev.

4. Pion Decay in Flight. The relative probability that a positive pion of mean life¹⁴ $\tau_\pi = 2.54 \times 10^{-8}$ sec. survives a time τ in its proper frame is $\exp(-\tau/\tau_\pi)$. Since a time $\tau = \tau(T_\pi)$ elapsed between the production and detection of the pion, the relative yield was corrected by the factor $\exp[\tau(T_\pi)/\tau_\pi]$. The value of $\tau(T_\pi)$ was obtained by integrating $d\tau$ over the pion's entire path length from the target, through the air and copper degraders, and to the third crystal. The pion decay-in-flight correction factor varied from 1.14 at 21.0 Mev to 1.07 at 113.5 Mev.

5. Nuclear Interaction of Pions. In passing through matter the pions could undergo nuclear interaction which may conveniently be classed as either multiple Coulomb scattering or nuclear attenuation.

a) Multiple Coulomb Scattering. Multiple Coulomb scattering in the energy degrader caused pions to be scattered out of the third crystal more frequently than into it owing to the limited aperture through which they had to pass in order to be detected. The formalism outlined in Appendix F was used in making the required calculation. The quantity obtained was $\overline{f(R)}$, which, for a given amount of degrader, was the ratio of the number of pions stopping owing to the limited aperture to the number that would have stopped if the aperture were unlimited. This calculation was repeated for each of the detection energies. The factor by which the number of detected pions was multiplied to get the number of incident pions is $1/\overline{f(R)}$, a quantity which varied from 1.00 at 21.0 Mev to 1.19 at 113.5 Mev.

b) Nuclear Attenuation. The term nuclear attenuation, as used here, includes all nuclear processes (e. g., inelastic scattering and diffraction scattering) except multiple Coulomb scattering that altered the pion's otherwise normal traversal of matter. Measurements²⁶ for the several contributing attenuation cross sections, although they are incomplete, suggest that the usual assumption of nuclear area, πR^2 , may be satisfactory for the total attenuation cross section, σ_{at} . The nuclear radius, R , was taken as $1.4 \times 10^{-13} A^{1/3}$ cm., where A is the atomic mass number. The correction factor for nuclear attenuation of pions traversing n nuclei per cm^2 in the pion energy degrader and one-half of the target, $\exp(n\sigma_{at})$, applied at each of the pion energies, varied from 1.01 at 21.0 Mev to 1.52 at 113.5 Mev. A correction for attenuation in the crystals--the same for all pion detection energies--did not have to be made, since only relative corrections were necessary.

6. Solid Angle. The solid angle subtended at the target by the face of the third crystal was not the same for both of the channels used. It can easily be shown that if ΔA is an element of area normal to a particle's orbit of radius of curvature ρ is a uniform magnet field and if ϕ is the total angle through which the particle turns in reaching ΔA , then the solid angle subtended at the center of the target per unit area of the detector face is $\Delta \Omega / \Delta A = (\rho^2 \phi \sin \phi)^{-1}$. A more complicated case occurs (as in this experiment) if the detector is a distance x outside the edge of the pole face, in which event the right-hand member²⁷ becomes $[\rho^2 (\phi + x/\rho)(1 + x/\rho \tan \phi) \sin \phi]^{-1}$. The ratio of the solid angles corresponding to the two channels was 1.42, the factor by which the yields obtained using the high-energy channel had to be multiplied in order to be normalized, in regard to solid angle, with respect to the yields obtained using the low-energy channel.

7. Muon Decay. The positive muon decays into a positron in accordance with the scheme²⁸ $\mu^+ \rightarrow \beta^+ + 2$ neutrinos, where the muon mean life^{13b} is 2.09×10^{-6} sec. and the energy spectrum of the positron has an upper limit of approximately 54 Mev. One wishes to know the probabilities that positrons appeared during the intervals that the gates were open, namely, $(2 \text{ to } 10) \times 10^{-8}$ sec. and $(19 \text{ to } 27) \times 10^{-8}$ sec. after the pion entered the telescope. It can be shown, by integrating the probability function for muon decay over the intervals during which the two gates were open, that the muons decaying during the gate intervals were not only

small in number (a few percent) but also almost equally divided between the two intervals.

A further reduction in the possibility of muon-decay effects was due to the fact that a positron in traversing the third crystal in the direction of the telescope could lose only about 2 Mev (compared with the 4-Mev loss by a muon). Consequently, no corrections were made for muon decay.

8. Summary. Table II gives a summary of all the multiplicative correction factors applied to the relative number of counts at each of the pion energies. These pion correction factors are independent of the proton energy. The mean pion production and detection energies are indicated by $T_{\pi}(p)$ and $T_{\pi}(d)$, and the subscripts on the multiplicative k factors (whose product is $\prod k$) denote relative target thickness (rtt), solid angle (sa), thick target (tt), energy dependence of detection interval (eddi), decay in flight (df), multiple scattering (ms), and nuclear attenuation (na).

Table II
Pion Correction Factors

| $T_{\pi}(p)$ | $T_{\pi}(d)$ | k_{rtt} | k_{sa} | $k_{tt} \cdot k_{eddi}$ | k_{df} | k_{ms} | k_{na} | $\prod k$ |
|--------------|--------------|-----------|----------|-------------------------|----------|----------|----------|-----------|
| 24.3 | 21.0 | 2.00 | 1.00 | 1.26 | 1.14 | 1.00 | 1.01 | 2.93 |
| 33.4 | 30.8 | 2.00 | 1.00 | 1.44 | 1.12 | 1.09 | 1.04 | 3.63 |
| 46.9 | 42.6 | 1.00 | 1.00 | 1.74 | 1.10 | 1.13 | 1.09 | 2.35 |
| 62.6 | 58.8 | 1.00 | 1.00 | 1.94 | 1.08 | 1.14 | 1.16 | 2.76 |
| 76.5 | 73.1 | 1.00 | 1.00 | 2.16 | 1.07 | 1.14 | 1.24 | 3.28 |
| 97.3 | 94.2 | 1.00 | 1.42 | 2.32 | 1.07 | 1.15 | 1.37 | 5.58 |
| 116.4 | 113.5 | 1.00 | 1.42 | 2.44 | 1.07 | 1.19 | 1.52 | 6.67 |

In Table III are listed all the correction factors by which each of the pion spectra (or the indicated part thereof) was multiplied. The energy of the proton beam leaving the degrader was $T_p(d)$; at the center of the target it was $T_p(t)$. The factors for nuclear absorption and diffraction are denoted by K_{na} and K_{nd} , and the effect of the excitation function on the targets of different thicknesses by K_e .

The pion and proton correction factors were appropriately combined and then applied to the raw data to obtain the final corrected data given in

Section IV.

Table III
Proton Correction Factors

| $T_p(t)$ | $T_p(d)$ | K_{nd} | T_π | | | |
|----------|----------|----------|-------------|-------------|-------|------|
| | | | K_{na} | | K_e | |
| | | | ≤ 30.8 | ≥ 42.6 | 21.0 | 30.8 |
| 335.6 | 340.0 | 1.000 | 1.007 | 1.014 | 0.97 | 0.98 |
| 313.4 | 318.0 | 1.002 | 1.075 | 1.082 | .97 | .98 |
| 294.2 | 299.0 | 1.005 | 1.138 | 1.146 | .95 | .96 |
| 264.2 | 269.3 | 1.014 | 1.243 | 1.252 | .95 | .95 |
| 235.2 | 240.7 | 1.027 | 1.348 | 1.358 | 0.95 | 0.93 |

C. Integration of Spectra

The relative total yield of positive pions at each proton energy was obtained by integrating the histogram of the corrected data; at the extremities of the spectra, however, it was necessary to resort to smooth-curve extrapolations (see Fig. 7). Accordingly, each of the areas and its standard deviation (due only to the statistics of counting) was determined by the expressions

$$A = \sum_i (\Delta T_{\pi i}) Y_i + A_L + A_H$$

$$\sigma_A^2 = \sum_i (\Delta T_{\pi i})^2 \sigma_{Y_i}^2 + \sigma_{A_L}^2 + \sigma_{A_H}^2,$$

where $Y_i \pm \sigma_{Y_i}$ is the relative yield at the i th pion production energy and hence the height of the i th rectangle whose width is $(\Delta T_{\pi i})$, and the indices L and H refer to the low- and high-energy extremities of the spectrum.

The results of these integrations are presented in Section IV.

D. Normalization for Absolute Values

The cross sections measured in this experiment were only relative values. The absolute scale was set by equating the area of the pion spectrum

for 336-Mev protons to the similar spectrum measured by Dudziak and mentioned in Section II-C-3. At a proton energy of 340 Mev he obtained the differential cross section $d\sigma(90^\circ) / d\Omega_{\text{lab}} = (3.35 \pm 0.12) \times 10^{-28} \text{ cm}^2/\text{sterad}$, where the error quoted is a standard deviation.

To take account of the different proton energies in the two experiments one used a power law to represent the excitation function in order to extrapolate the emulsion data. (The power law used was of the form mentioned in Section III-B-2-b, and was the least-squares fit to the five integrated pion energy spectra of the present experiment.) Finally, account was taken of the errors in both the emulsion and counter data in the determination of the error of the absolute scale for the excitation function.

IV. RESULTS

The relative differential cross section for positive pions produced at 90° in the reaction $p + C \rightarrow \pi^+$ is given in Table IV and Fig. 7 as a function of pion and proton energies. The errors shown are the standard deviations due to statistics of counting. The curves drawn through the spectra have no theoretical significance; they simply indicate the extrapolations used in the integration of the spectra.

Table IV

Relative Differential Yield at 90° for $p + C \rightarrow \pi^+$

| T_p \ T_π | Relative $\frac{d\sigma(T_p, T_\pi, 90^\circ)}{d\Omega dT_\pi}$ | | | | | | |
|-----------------|---|--------------------|--------------------|---------------------|--------------------|--------------------|--------------------|
| | 24.3 | 33.4 | 46.9 | 62.6 | 76.5 | 97.3 | 116.4 |
| 336 | 10.00 ± 0.39 | 9.88 ± 0.60 | 8.84 ± 0.24 | 6.34 ± 0.43 | 5.24 ± 0.43 | 1.63 ± 0.36 | 1.28 ± 0.38 |
| 313 | 8.89 ± 0.58 | 9.00 ± 0.71 | 7.15 ± 0.49 | 3.79 ± 0.38 | 3.38 ± 0.51 | 1.48 ± 0.43 | -- -- |
| 294 | 4.28 ± 0.69 | 4.92 ± 0.81 | 3.96 ± 0.52 | 3.42 ± 0.60 | 2.66 ± 0.58 | -- -- | -- -- |
| 264 | 3.73 ± 0.67 | 3.49 ± 0.84 | 2.91 ± 0.51 | 2.06 ± 0.64 | 1.97 ± 0.90 | -- -- | -- -- |
| 235 | 2.38 ± 0.69 | 2.16 ± 0.86 | 1.72 ± 0.58 | -0.21 ± 1.28 | -- -- | -- -- | -- -- |

The results of integrating (as described in Section III-C) over the pion energy spectra are presented in Table V and Fig. 8. The curve shown is the power law $Y(T_p) \sim (T_p - T_0)^b$, where T_0 was arbitrarily taken to be the absolute threshold (~ 150 Mev) for this reaction. A least-squares calculation gave $b = 2.5 \pm 0.6$, where the standard deviation of b was calculated by external consistency (~ 50 percent larger than that calculated by internal consistency).

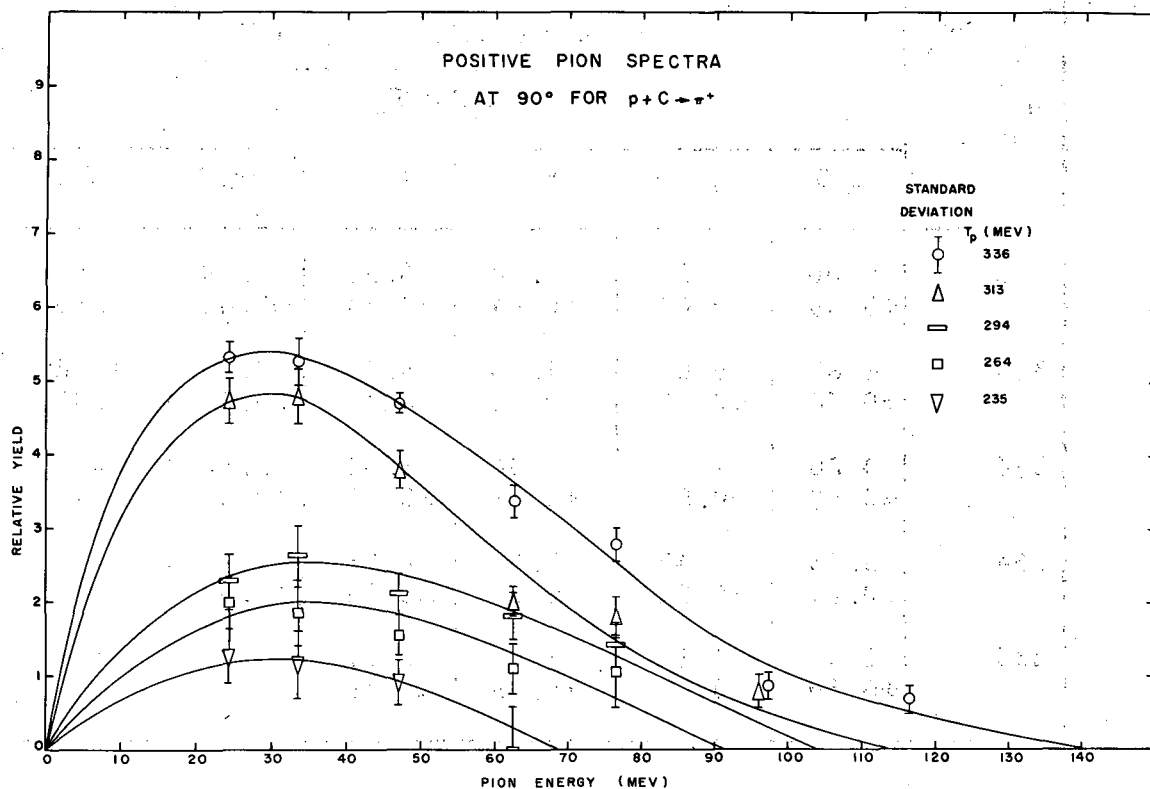


Fig. 7 - Positive pion spectra at 90° for $p + C \rightarrow \pi^+$ in the proton energy interval 235 to 336 Mev. The curves shown have no theoretical significance; they simply indicate the extrapolations used in the integration of the spectra.

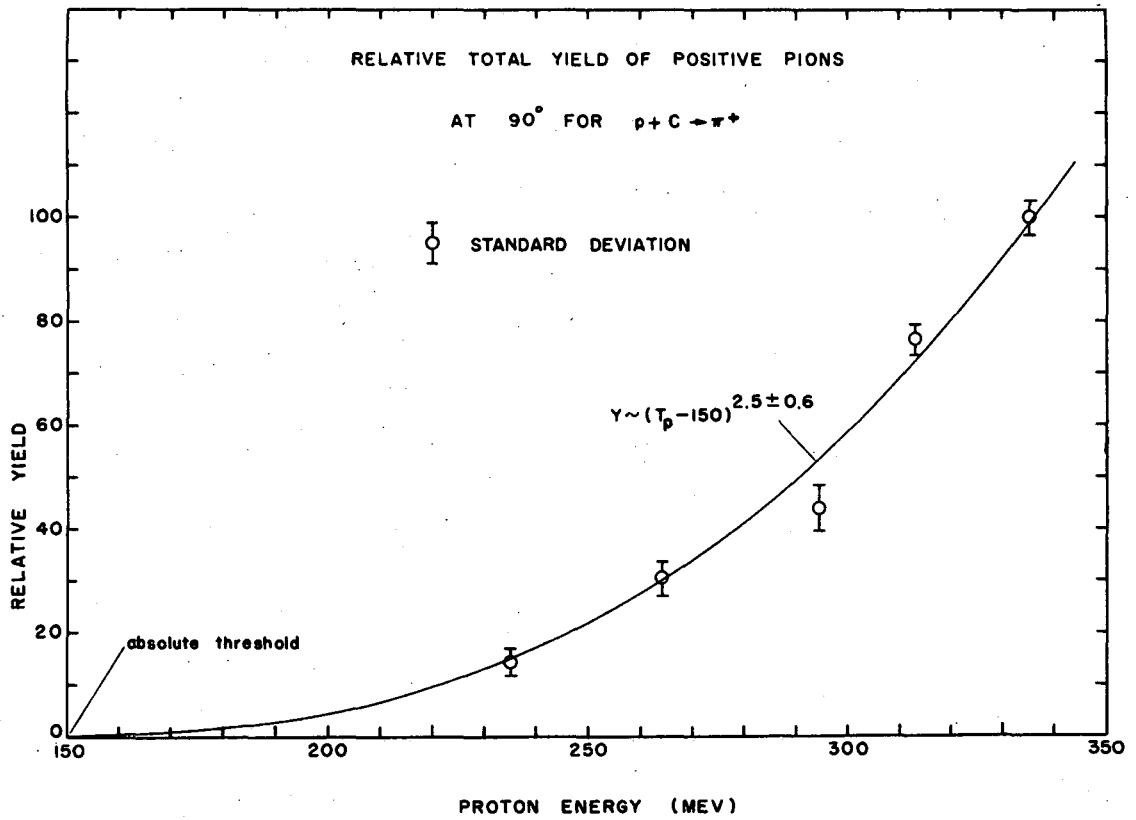


Fig. 8 - Excitation function for positive pions at 90° for $p + C \rightarrow \pi^+$.
The curve shown is the assumed power law $Y(T_p) \sim (T_p - T_0)^b$,
where T_0 was arbitrarily taken to be the absolute threshold
for this reaction; the exponent was determined by least squares.

Table V

Relative Integrated Yield at 90° for $p + C \rightarrow \pi^+$

| T_p (Mev) | 235 | 264 | 294 | 313 | 336 |
|--|-------------------|-------------------|-------------------|-------------------|--------------------|
| Relative $\frac{d\sigma(T_p, 90^\circ)}{d\Omega_{lab}}$ | 14.7 ± 2.4 | 30.5 ± 3.4 | 43.9 ± 4.3 | 76.0 ± 3.0 | 100.0 ± 3.6 |

The absolute scale for the excitation function was set (as described in Section III-D) at $T_p = 336$ Mev to be $d\sigma(336, 90^\circ)/d\Omega_{lab} = (3.20 \pm 0.16) \times 10^{-28}$ cm²/sterad.

V. DISCUSSION

The excitation function measured in this experiment is shown in Fig. 9 with the three points at higher proton energies obtained by Passman et al.⁶ The scheme used for normalization was to put their 345-Mev point on the power law curve determined by the lower five points.

It is pointed out by Passman et al. that the peaks of their pion spectra shift to higher pion energies as the proton energy is increased. In the present experiment the peak of the pion spectrum for 336-Mev protons falls in the neighborhood of 30 Mev; no noticeable shift occurs for lower proton energies.

Complete understanding of pion production from a complex nucleus (such as carbon) bombarded by a nucleon will not be reached until a satisfactory detailed analysis can be made in terms of elementary nucleon-nucleon collisions. Such an analysis is not only tedious but also complicated. Some of the more important considerations are concerned with the nature of the nucleon-nucleon collisions (e. g., end products, angular distribution, and excitation function), the internal nuclear momentum distribution (e. g., Fermi degenerate gas, gaussian, and Chew-Goldberger), the balance of momentum and energy (i. e., to what extent the nucleus takes part in the collision), and the interaction of the pions with nuclear matter (i. e., scattering and reabsorption). Despite the complexity of the problem there have been attempts by Henley,²⁹ Passman et al.,⁶ Neher,³⁰ and Leonard.⁵

The calculation that can most easily be compared with the present data is that of Passman et al. Their principal assumptions are a gaussian nuclear momentum distribution and a $p + p \rightarrow \pi^+$ production process characterized in the c. m. system by (1) a $\cos^2 \theta$ angular distribution, (2) the pion's receiving all available kinetic energy T_{\max} , and (3) an excitation function $\sim T_{\max}^2$. Their calculation predicts an increase in the 90° differential cross section of ~ 1.5 in the energy interval 345 to 380 Mev. The increase predicted by the power law determined by the present experiment is also 1.5. This agreement, however, must not be taken too seriously, owing to the various approximations made in the calculations and to possible experimental errors.

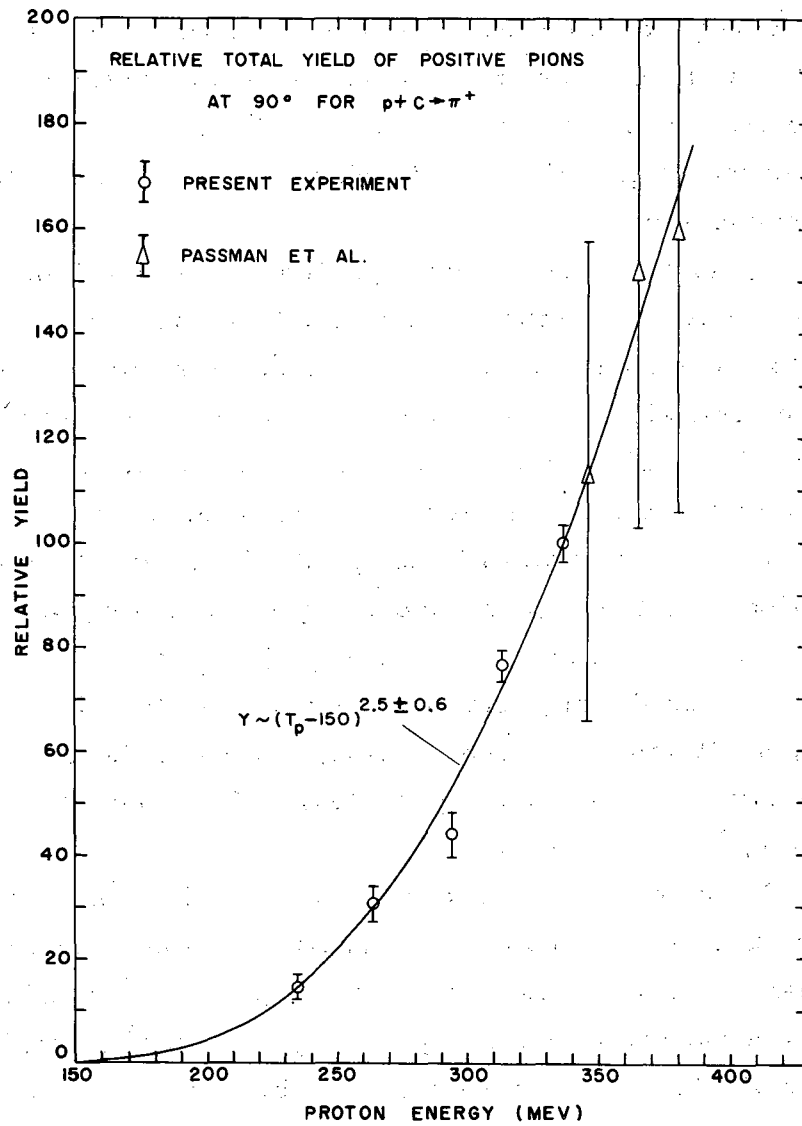


Fig. 9 - Comparison of the present data and those obtained by Passman et al. for the excitation function for positive pions at 90° for $p + C \rightarrow \pi^+$. Their 345-Mev point was arbitrarily placed on the power law curve determined by the present experiment.

Finally, it may be interesting to note the similarity in the shapes of the experimental excitation functions for positive, negative, and neutral pions produced in carbon bombarded by protons. In Fig. 10 the π^+ data are those of this experiment (integrated energy spectrum at 90°), the π^- data are those of Jones and White¹ (2 to 10 Mev, 0 to 45°), and the π^0 data are those of W. Crandall,³¹ who measured the total production cross section at each proton energy. The method used to normalize the three sets of data was to require the power laws representing the π^- and π^0 data to intersect (at the highest proton energy) the power law representing the π^+ data. It should be emphasized, however, that the three quantities measured in these experiments are different in regard to angles, etc; therefore, the agreement (within statistics) of the exponents for the power laws fitting the data may be fortuitous.

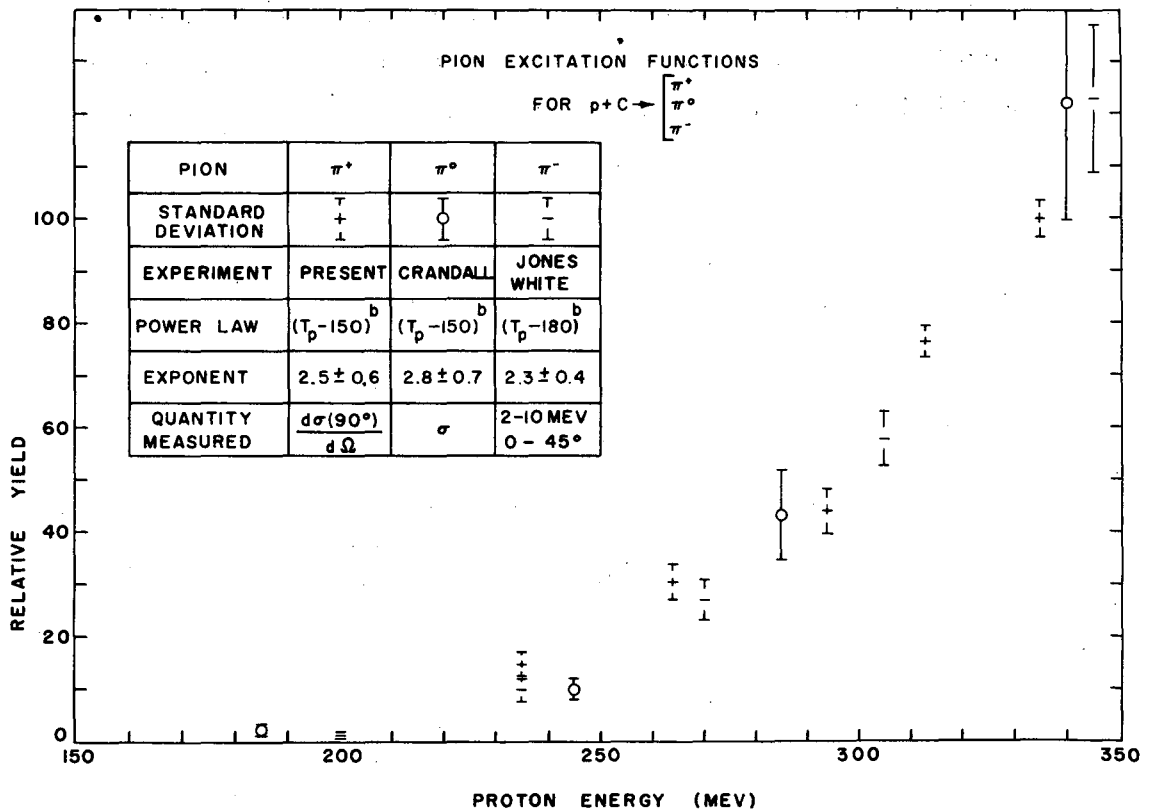


Fig. 10 - Comparison of the shapes of the excitation functions for positive, neutral, and negative pions produced in carbon bombarded by protons. The power laws for the π^0 and π^- data were normalized (at the highest proton energies) to the power law for the π^+ data.

VI. ACKNOWLEDGMENTS

I wish to express my appreciation to Professor Chaim Richman for suggestions and support throughout my graduate research work. To Jack Merritt I am indebted for much material aid and many profitable discussions. Sincere thanks are given to Drs. Alvin G. Schulz and Mark J. Jakobson for their guidance in the early stages of my work with electronics, and to Dr. R. S. White for constant encouragement. I wish to thank James Vale, Lloyd Houser, and the crew members for their help and cooperation during the cyclotron bombardments.

VII. APPENDICES

A. Smoothing of Background Fluctuations

The use of two sets of delayed-coincidence circuits, with an interchange of delay cables on successive units of integrated beam, had a 'smoothing' effect on the background fluctuations due to beam intensity fluctuations. Suppose that, per unit of integrated beam, set A counted P pions and B background particles during an integration time of t ; set B counted with a fractional efficiency f of set A. After two units of integrated beam requiring t and $t \pm \Delta t$ as integration times, the data would have taken the following form:

| Set A | | Set B | |
|-----------------------|-------|------------------------------|-------|
| Counts | Delay | Counts | Delay |
| $P + B$ | short | fB | long |
| $B(1 \mp \Delta t/t)$ | long | $f[P + B(1 \mp \Delta t/t)]$ | short |

The difference between the total number of short-delay counts and the total number of long-delay counts for the two units of integrated beam is $P(1 + f) \pm [B(1 - f) \Delta t/t]$, a quantity that should be the total number of pions for the two units of integrated beam. The term in square brackets, however, is due to background counts that were erroneously mixed in with the pion counts owing to a difference in integration times when there was a difference in efficiencies of the two sets. It is noted that this error vanishes for either equal integration times ($\Delta t = 0$) or equal efficiencies ($f = 1$) of the two sets. If, for example, $B/P = 1/2$ and $\Delta t/t = 1/5$, then the fractional errors for the two cases in which $f = 0$ (only one set) and $f = 4/5$ are 10 percent and 1 percent, respectively. No corrections were made because, in practice, conditions were somewhat more favorable than in the numerical example of $f = 4/5$.

B. Description of Electronics

A block diagram of the electronics used is shown in Fig. 3. Included here are the two sets of pion identification circuits and the

distributed amplifiers;³² also shown are the linear amplifiers and scalers, which were standard UCRL counting-area equipment. The dotted rectangles indicate that the enclosed circuits, whose circuit diagrams are shown in Figs. 11 and 12, were built on a single chassis.

This $\pi^+ - \mu^+$ delayed-coincidence equipment, as already mentioned, differed from Jakobson's original in two respects: (1) three crystals (instead of two) were used in the telescope, and (2) two sets of circuits (instead of one) were used in making the delayed coincidence. The advantages of the telescope described here were that plateaus (discussed in Appendix C) were obtained for the pions passing through the first two crystals and that pions of lower energy could be detected. (Thinner crystals necessitated new distributed amplifiers DA-1, 2 with higher gains.) The advantages of the two sets of circuits were discussed in Section II-C-2.

For each of the distributed amplifiers in Table VI one finds listed the gain corresponding to its maximum output into the load occurring in the circuit; also indicated is the design bandwidth.

Table VI
Distributed Amplifier Characteristics

| Distributed Amplifier | Gain | Max. volts out | Load (ohms) | Bandwidth (Mc) |
|-----------------------|------|----------------|-------------|----------------|
| DA-1, 2 | 40 | (+) 8 | 190 | 175 |
| DA-IA, B | 3.5 | (-) 6 | 390 | 200 |
| DA-3A, B | 6.5 | (+) 12 | 360 | 200 |

The distributed coincidence circuits I and II were patterned after the original design of Wiegand.³³ The resolution of CI was measured with two different pulse sources. On the one hand, a pulse of $\sim 1.0 \times 10^{-8}$ sec. duration (at its base) from a pulse generator was split and sent to both inputs of the distributed amplifiers DA-1, 2 preceding CI.

The latter's output pulse was measured as a function of the delay introduced in one side of the input. The full-width at half-maximum of the resolution curve thus obtained was $\sim 0.8 \times 10^{-8}$ sec. On the other hand, for the pulses caused by protons passing through the first two crystals, mounted at the end of 28-inch light pipes, the resolution was only about half as good. The ratio of the CI output voltage for signals in both inputs to the output for a signal in one input was larger than ten.

The delay cables between CI and the GG's, as well as all other cables carrying $\sim 10^{-8}$ sec. pulses, were of the type RG-63/U (125 ohm characteristic impedance), which provided a delay of $\sim 0.4 \times 10^{-8}$ sec. per meter of cable. The frequent alternations between the short- and long-delay cables were facilitated by coaxial cable switches which could be remotely operated by means of 110-volt relays.

The gate generator, the most crucial element in the entire circuitry, was a cathode-coupled univibrator which, when triggered by a $\sim 10^{-8}$ -sec. input signal of ≥ 6 volts, gave a rectangular output having a rise time $< 10^{-8}$ sec., a height of $\sim +10$ volts, and a duration of $\sim 8 \times 10^{-8}$ sec. at 0.8 full height. To obtain a gate having these characteristics it was necessary to select tubes rather carefully (see reference 14b for important hints). In order to monitor the number of gates generated a small fraction of the gate signal was taken from a voltage divider on the cathode follower following the gate generator, adequately inverted with a passive pulse transformer, sent through a linear amplifier, and finally scaled.

The pulses entering sets A and B from the third photomultiplier were of opposite polarity since the signals were taken from the plate and the last dynode, respectively. Consequently, it is strictly the set A circuit diagram that is shown in Fig. 12; set B differs, however, only in an input tube for which a phase inverter (of the type shown in Fig. 11) replaces the cathode follower shown.

Discrimination of the output signals from CII was performed by a trigger circuit which gave a 2 μ sec. rectangular pulse each time it was tripped. These latter pulses, after passing through a linear amplifier, were recorded on a scaler. All the scalers were allowed to count (by means of a synchronized gating signal from standard auxiliary circuits)

during only a small selected time interval centered about a synchrocyclotron fm pulse. Mechanically operated switches enabled one to allow the scalers to count for any desired amount of integrated beam.

C. Voltages, Plateaus, and Detection Efficiencies

1. Plateaus for Photomultipliers Nos. 1 and 2. The procedure used to obtain the plateau curves shown in Fig. 4 for the first two photomultipliers was to determine the pion counting rate as a function of the voltage applied to one of the photomultipliers while holding all other voltages constant. The pion counting rates shown are those obtained by combining the counts from the two sets A and B. The curves shown* do not statistically differ in shape from those obtained by plotting the individual counting rates of the two sets A and B. The significance of the plateau regions of Fig. 4 is that every pion entering the telescope and stopping in the third crystal caused a gate to be generated, provided the photomultipliers were operated somewhere in the plateau region.

2. Photomultiplier No. 3 Voltage. After the operating voltages were selected for photomultipliers Nos. 1 and 2, an attempt was made to find a plateau region for photomultiplier No. 3. A satisfactory region over which the pion counting rate was voltage-independent was not found; consequently, it was necessary to resort to a different method, such as that discussed below, for selecting the operating voltage of photomultiplier No. 3.

The experimental setup⁷ used during the search for voltage plateaus for the photomultipliers, Nos. 1 and 2 as well as No. 3, was similar to that already described except that the pions to be detected were emitted from a $(\text{CH}_2)_n$ (instead of carbon) target at 0° (instead of 90°) with respect to the beam. An appropriate setting of the magnetic field allowed a relatively high flux of approximately 62-Mev positive pions, produced in the two-body reaction²³

* Plateau curves for the first two photomultipliers, very similar to those shown here, were also obtained³⁴ under background conditions quite different from those existing in the cave at the synchrocyclotron. In this experimental arrangement the scintillation counter telescope accepted positive pions emitted from a target at 140° with respect to the 320-Mev bremsstrahlung beam of the Berkeley synchrotron.

$p + p \rightarrow \pi^+ + d$, to pass down the channel, enter the telescope, stop in the third crystal, and hence be detected--provided the correct amount of pion energy degrader was placed in front of the telescope. When the degrader was removed this high flux of pions passed entirely through the three crystals and, therefore, was not detected.

It was under this arrangement of no pion degrader that, after determining the 'pion' counting rate as a function of the photomultiplier No. 3 voltage, one selected the operating voltage for photomultiplier No. 3. In the interval 1200 to 1350 volts one obtained a few counts compatible with the number of pions that could scatter off the channel walls and stop in the third crystal. For higher voltages the counting rate began to increase rather rapidly. Consequently, the selected operating voltage was one that lay below the break in the counting-rate curve. To verify that the selected voltage was reasonable, one replaced the pion energy degraders and ran a mean life on the particles by varying the length of the short-delay cable. The value obtained was in agreement with the published values^{14, 24} for positive pions. A complete discussion concerning the validity of detection is given in Section II-C-3.

Several possible reasons may be given for the lack of a plateau region for the positive-pion detection efficiency as a function of the photomultiplier No. 3 voltage. First, the light-collection efficiency may have varied over the crystal. Second, the ratio of the number of muons having a partial path length to those having either a complete or partial path length in the third crystal was ~ 0.18 (this number takes into account pions stopping just outside the third crystal as well as those stopping inside). Third, the relatively long light pipes between the crystals and photomultipliers could have caused statistical fluctuations³⁵ in the size of the muon pulses in addition to those occurring in the absence of the light pipes. Each of the above-mentioned factors would have contributed a finite slope to any a priori expected plateau.

The increase in the counting rate (versus photomultiplier No. 3 voltage) beyond the number of pions known to be present requires an explanation. It has been suggested that a proton entering the telescope and stopping in the third crystal could have given a pulse sufficiently large to saturate the amplifiers. The resulting output pulse could have

been so broadened that its tail would have fallen into the short-delayed gate (although not into the long-delayed gate). Thus, CII would have given a net number of counts at the short delay. To show that this condition was not present at the operating voltage selected for photomultiplier No. 3 and, further, that the detection equipment was not plagued by 'satellite' pulses believed to follow a main pulse in a photomultiplier,³⁶ the following test was performed.

The facilities of the Berkeley 32-Mev proton linear accelerator were used. Since these protons were not sufficiently energetic to pass through the entire counter telescope, the following expedient was employed. Approximately 15-Mev protons were allowed to enter only the third crystal of the telescope. In order that a gate would be generated each time a proton entered the crystal, the signal taken off the last dynode of photomultiplier No. 3 and normally sent to CII-B was, instead, split and sent to CI. The signal from the plate of photomultiplier No. 3 was sent as usual to CII-A (set B of the detection electronics was not used in this test). Set A was run on the short- and long-delay cables for equal amounts of integrated beam; the delay cable was frequently alternated. During the time that a total of 1.85×10^5 gates were generated, 28 and 35 coincidences were made, respectively, at the short and long delays. One thus concludes that, whatever the nature of the event that was causing the coincidences, it was equally likely (within the statistics obtained) to occur at long and short delays. It is extremely probable, furthermore, that most if not all of the coincidences obtained were of an accidental nature owing to fluctuations in the beam intensity. Finally, it is noted that, under typical conditions for the experiment described in this paper, a total number of pions ranging from 90 to 570 was detected for 1.85×10^5 gates. It is thus concluded that any effects of the nature described in the previous paragraph were negligible.

3. Detection Efficiency. The absence of a plateau region required some method for checking on the constancy of the detection efficiency over the duration of a single run (two or three days) and also from run to run. In the first case, it was found that no systematic trend could be detected in the data obtained by cycling a group of pion and proton energies several times in the course of a single day; the fluctuations in counts on various

cycles were entirely compatible with the expected statistical fluctuations. In the second case, the detection efficiency appeared to be statistically different on different runs. Thus, it was necessary to normalize the detection efficiency on one run to that on another. These matters of consistency and normalization are discussed in detail in Section III-A and Appendix D.

It is estimated (from comparisons with nuclear emulsion data) that the absolute detection efficiency of the $\pi^+ - \mu^+$ delayed-coincidence equipment was 10 to 15 percent for all the positive pions entering the telescope and stopping in the third crystal.

D. Detection Efficiency Normalization Formula

The problem of normalizing the detection efficiencies of different runs will be considered in some detail. Let it be supposed that on two runs the relative numbers of pions detected per unit of integrated beam at the i th pair of proton and pion energies (hereafter referred to as the i th point) were $n_i \pm \sigma_{n_i}$ and $N_i \pm \sigma_{N_i}$, where σ_i is the standard deviation. The problem is to find the constant factor k such that the set of values $k(N_i \pm \sigma_{N_i})$ will be in best agreement with the set $(n_i \pm \sigma_{n_i})$. It is assumed that the criterion of best agreement is satisfied by application of the principle of least squares, which leads to the most probable value for the constants entering an equation of an assumed form. In applying the principle to the present problem one requires

$$\sum_i w_i (n_i - kN_i)^2 = \text{minimum},$$

where w_i , the weight assigned to the i th point, is arbitrarily taken inversely proportional to the sum $(\sigma_{n_i}^2 + \sigma_{N_i}^2)$. (It turns out that k is rather insensitive to the quantity selected for the weight w_i .) Solving for k one obtains

$$k = \frac{\sum_i w_i n_i N_i}{\sum_i w_i N_i^2},$$

and applying the general formula for propagation of errors one obtains for the standard deviation of k ,

$$\sigma_k^2 = C^2 \sum_i w_i^2 \left[(N_i \sigma_{n_i})^2 + (M_i \sigma_{N_i})^2 \right],$$

where $\bar{C}^{-1} = \sum_j w_j N_j^2$, $M_i = 2kN_i - n_i$; and for the standard deviation of the product kN_m ,

$$\sigma_{kN_m} = \left[1 + \frac{(\sigma_k / k)^2}{(\sigma_{N_m} / N_m)^2} - G_m \right]^{1/2} k \sigma_{N_m},$$

where the term G_m , a consequence of the dependency of k on N_m , is given by $G_m = 2CM_m N_m w_m k^{-1}$.

E. Thick-Target Correction Factor

Considered here is the derivation of the correction factor which took into account the difference in energy intervals for pion production and detection due to a thick target. Figure 13 explains the notation used. Those two pions which were produced at a distance x from the front of the target and which stopped at the back and front of the third crystal in the telescope were separated in energy by an amount $(\Delta T_\pi)_x$ at the plane x in the target, by an amount $(\Delta T_\pi)_d$ at the front face of the degrader placed in front of the telescope, and by an amount $(\Delta T_\pi)_{f1}$ at the front face of the first crystal in the telescope. The quantity $(\Delta T_\pi)_x$, which was dependent on the position of pion production in the target, had to be averaged over the target to obtain $\overline{(\Delta T_\pi)_x}$. To obtain this quantity one may write

$$T_\pi(R_{x, b3}) = T_\pi(R_{x, f3} + R_o),$$

where $R_{x, b3} = R_{x, f3} + R_o$.

Expanding and dropping terms greater than second order, one gets

$$(\Delta T_\pi)_x \equiv T_\pi(R_{x, b3}) - T_\pi(R_{x, f3}) = \left[\frac{dT_\pi}{dR_{f3}} \right]_x R_o + \left[\frac{d^2 T_\pi}{dR_{f3}^2} \right]_x R_o^2.$$

SCHEMATIC FOR TARGET, DEGRADER, & CRYSTALS

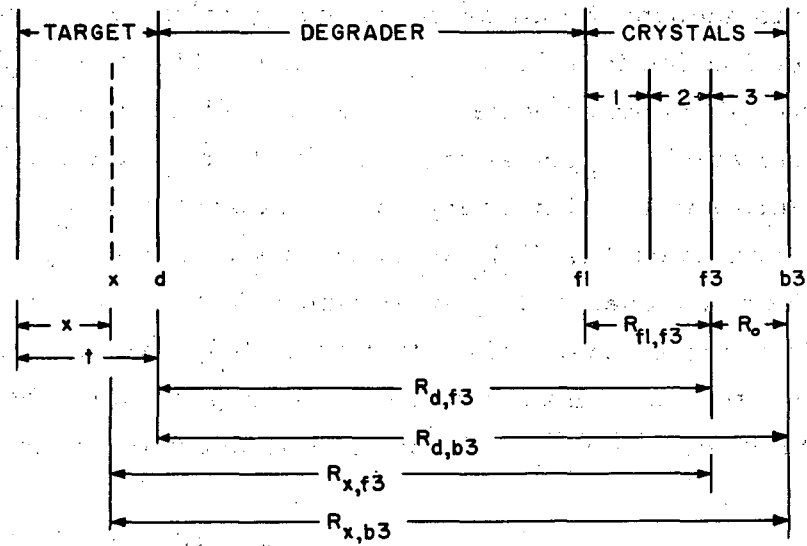


Fig. 13 - Schematic diagram of the target, pion energy degrader, and crystals used in the derivation of a thick-target correction factor.

An average over a target of thickness t yields

$$\begin{aligned} \overline{(\Delta T_\pi)_x} &= \frac{1}{t} \left[R_o \int_{x=t}^o \left[\frac{dT_\pi}{dR_{f3}} \right]_x dx + R_o^2 \int_{x=t}^o \left[\frac{d^2 T_\pi}{dR_{f3}^2} \right]_x dx \right] \\ &= \frac{R_o}{t} \left[\left[T_\pi^{f3}(o) - T_\pi^{f3}(t) \right] - R_o \left\{ \left[\frac{dT_\pi}{dR_{f3}} \right]_t - \left[\frac{dT_\pi}{dR_{f3}} \right]_o \right\} \right] \end{aligned}$$

The largest ratio of the second- and first-order terms occurred at 21.0 Mev, where it was 0.18.

The ratio of $(\Delta T_\pi)_d$ and the above derived $\overline{(\Delta T_\pi)_x}$ is the correction factor that took into account the difference in energy intervals for pion production and detection due to a thick target.

F. Multiple Coulomb Scattering

1. Distribution Functions. A summary is presented here of the formulae for the lateral and angular distribution of charged particles which undergo multiple Coulomb scattering. The distribution function that was derived by Eyges,²⁵ and which takes into account to a good approximation the energy loss suffered by the incident particle owing to ionizing collisions, is

$$F(t, y, \theta) = \frac{(B)^{-1/2}}{4\pi} \exp - \left[\frac{A_o y^2 - 2A_1 y \theta + A_2 \theta^2}{4B} \right],$$

where
$$A_m(t) = \int_0^t \frac{(t-\eta)^m}{W^2(\eta)} d\eta, \quad m = 0, 1, 2;$$

the projected lateral displacement y and the projected angular displacement θ are measured in any plane containing the incident particle; t is the depth of penetration in the degrader; $B = A_o A_2 - A_1^2$; $W = 2p/E_s$; p and β are the momentum and velocity of the particle; and $E_s = 21$ Mev.

The distribution function into which $F(t, y, \theta)$ is transformed at a distance L beyond the rear face of the degrader is $F(t, L; Y, \theta)$, obtained by

the substitution $y = Y - L\theta$. The lateral distribution (independent of angle) resulting from integration over θ is

$$F(t, L; Y) = \frac{(\pi C)^{-1/2}}{2} \exp - \left[\frac{Y^2}{4C} \right],$$

where $C = A_0 L^2 + 2A_1 L + A_2$.

The projected lateral distribution in the (t, X) plane is described, owing to symmetry, by the same function F that describes it in the (t, Y) plane. Since deflections in the two orthogonal directions X and Y are independent of each other, the probability of a particle's suffering a lateral displacement with components X and Y is the product

$$F(t, L; X)F(t, L; Y) \equiv F(t, L; R), \quad \text{where } R \equiv (X, Y).$$

A useful interpretation of the function $F(t, L; R')$ is that it also gives the probability that a particle, having the lateral coordinates $(X', Y') \equiv R'$ upon entering the degrader, will be scattered so that it will strike the point $X = Y = 0$ in the detector plane (the plane at a distance L beyond the degrader). Generalizing, one writes

$$F(t, L; R', R) = \frac{1}{4\pi C} \exp - \left[\frac{(X' - X)^2 + (Y' - Y)^2}{4C} \right]$$

as the probability that a particle entering the degrader at the point R' will strike the detector plane at R .

2. Loss Due to an Aperture. If an aperture in front of the degrader restricts the lateral extent of an incident beam of charged particles, then the point R in the detector plane will receive only a fraction $f(R)$ of the particles it would without restriction. This fraction is

$$f(R) = \iint_A F(t, L; R', R) dR',$$

where $dR' = dX' dY'$, and the 'source function' $F(t, L; R', R)$ is integrated over the entire aperture A . The fractional number of particles received by the entire detector is

$$\overline{f(R)} = D^{-1} \iint_{\text{det}} f(R) dR,$$

where the integration is extended over the entire detector whose area is

$$D = \iint_{\text{det}} dR.$$

For the case in which a rectangular aperture is aligned with its edges parallel to those of the detector (as in this experiment), $f(R)$ reduces to a simpler expression, $f(X)f(Y)$, where $f(X)$, given by

$$f(X) = \frac{(\pi C)^{-1/2}}{2} \int_{A(X')} \exp - \left[\frac{(X' - X)^2}{4 C} \right] dX' ,$$

is independent of Y ; $A(X')$ is the X' extent of the aperture corresponding to X . The expression for $f(Y)$ is analogous. (The point is that $f(X)$ would be an implicit function of Y if X' depended on Y .) The function $f(X)$ may be interpreted as the fractional number of particles that would be received by the point X if the aperture of half-width X' extended without limit in the Y' direction.

The evaluation of $\overline{f(R)}$ for this case of a rectangular aperture may now be carried out rather easily to any desired accuracy by dividing the area D of the detector into a rectangular grid network whose ij th cell has an area D_{ij} . By defining f_i (or f_j) as the average value of $f(X)$ (or $f(Y)$) over the X (or Y) extent of the i th (or j th) column (or row) of cells, one may superimpose upon the grid network a multiplication table which, having f_i (or f_j) as the horizontal (or vertical) heading, will have products $f_i f_j \equiv f_{ij}$, the fractional number of particles received by the ij th cell. The fractional number of particles received by the entire detector is then

$$\overline{f(R)} \simeq \overline{f_{ij}} = D^{-1} \sum_i \sum_j f_{ij} D_{ij}$$

since

$$D = \sum_i \sum_j D_{ij} .$$

In applying the above formulism to calculating the multiple Coulomb scattering correction for pions, one took for L the distance from the pion degrader to the middle of the third crystal (multiple scattering in the first two crystals was negligible). At each of six points across the

half-width of the third crystal the value of $f(X)$ was calculated for the X' that corresponded to that point; near the center (or edge) of the third crystal the channel (or first crystal) provided the effective aperture. Using the curve drawn through the plotted values of $f(X)$, one obtained f_i by inspection. The values of f_j were taken as equal to those of f_i since there was effectively a fourfold symmetry for the telescope and channel.

REFERENCES

1. S. B. Jones and R. S. White, Relative Yield Functions for π^- -Mesons from Carbon, Phys. Rev. 78, 12 (1950).
S. B. Jones and R. S. White, Yield of Negative π -Mesons Produced by High Energy Protons as a Function of Proton Energy, Phys. Rev. 76, 588A (1949).
2. C. Richman and H. A. Wilcox, Production Cross Sections for π^+ and π^- Mesons by 345-Mev Protons on Carbon at 90° to the Beam, Phys. Rev. 78, 496L (1950).
C. Richman, M. Weissbluth, and H. A. Wilcox, Production Cross Sections for π^+ - and π^- -Mesons by 340-Mev Protons on Carbon and Lead at 90° to the Beam, Phys. Rev. 85, 161 (1952).
3. W. F. Dudziak, private communication.
4. W. F. Dudziak, Measurement of the Production Cross Section of Negative Mesons in Carbon by 341-Mev Protons, Phys. Rev. 86, 602A (1952).
5. S. L. Leonard, Yield of Charged Pions at 180° to the Beam by 340-Mev Protons on Carbon, Thesis, University of California Radiation Laboratory Report No. UCRL-2210, May, 1953.
6. S. Passman, M. M. Block, and W. W. Havens, Jr., Excitation Function for Charged π -Meson Production in Hydrogen and Carbon by 345- to 380-Mev Protons, Phys. Rev. 88, 1247 (1952).
7. A. G. Schulz, The Excitation Function for π^+ -Mesons Produced in P-P Collisions at 0° to the Beam, Thesis, University of California Radiation Laboratory Report No. UCRL-1756, May, 1952.
A. G. Schulz, D. Hamlin, M. J. Jakobson, and J. Merritt, The Excitation Function for π^+ Mesons Produced in P-P Collisions, Phys. Rev. 87, 219A (1952).
8. C. E. Leith, A Multiple Scattering Deflector for the 184-inch Cyclotron, Phys. Rev. 78, 89A (1950).
9. R. E. Richardson, W. P. Ball, C. E. Leith, Jr., and B. J. Moyer, Nuclear Elastic Scattering of High Energy Protons, Phys. Rev. 86, 29 (1952).
R. E. Richardson, Elastic Scattering of 340-Mev Protons, Thesis, University of California Radiation Laboratory Report No. UCRL-1408, July, 1951.

10. O. Chamberlain, E. Segrè, and C. Wiegand, Experiments on Proton-Proton Scattering from 120 to 345 Mev, *Phys. Rev.* 83, 923 (1951).
11. W. A. Aron, The Passage of Charged Particles Through Matter, Thesis, University of California Radiation Laboratory Report No. UCRL-1325, May, 1951.
W. A. Aron, B. G. Hoffman, F. C. Williams, Range-Energy Curves (Second Revision 1949) AECU-663.
12. T. J. Thompson, The Effect of Chemical Structure on Stopping Powers for High Energy Protons, Thesis, University of California Radiation Laboratory Report No. 1910, August, 1952.
- 13a. F. Rasetti, Disintegration of Slow Mesotrons, *Phys. Rev.* 60, 198 (1941).
- 13b. L. W. Alvarez, A. Longacre, V. G. Ogren, and R. E. Thomas, Electrical Detection of Artificially Produced Mesons, *Phys. Rev.* 77, 752A (1950).
- 13c. J. Steinberger and A. S. Bishop, The Detection of Artificially Produced Photo-Mesons with Counters, *Phys. Rev.* 78, 493L (1950).
- 14a. M. Jakobson, A. Schulz, and J. Steinberger, Detection of Positive π -Mesons by π^+ Decay, *Phys. Rev.* 81, 894L (1951).
- 14b. M. Jakobson, A. Schulz, J. Steinberger, Detection of Positive π Mesons by π^+ Decay, University of California Radiation Laboratory Report No. UCRL-1061, December, 1950.
15. D. Hamlin, M. Jakobson, J. Merritt, and A. Schulz, π^+ -Meson Production Cross Section as a Function of Atomic Number, *Phys. Rev.* 84, 857L (1951).
- 16a. R. S. White, M. J. Jakobson, A. G. Schulz, The Production of Charged Photomesons from Deuterium and Hydrogen. I, *Phys. Rev.* 88, 836 (1952).
- 16b. M. J. Jakobson, A. G. Schulz, and R. S. White, Production of Charged Photomesons from Helium, Hydrogen-Helium Ratios. II, *Phys. Rev.* 91, 695 (1953).
17. J. Merritt, Cross Sections for the Production of π^+ Mesons by 335-Mev Protons as a Function of Atomic Number, Thesis, University of California Radiation Laboratory Report No. 2424, November, 1953.
18. C. M. G. Lattes, G. P. S. Occhialini, and C. F. Powell, Observations on the Tracks of Slow Mesons in Photographic Emulsions, *Nature* 160, 453 (1947).

19. W. H. Barkas, Meson Masses and Energetics of Meson Decay, Amer. Jour. of Phys. 20, 5 (1952).
20. C. Wiegand, Measurement of the Positive π -Meson Lifetime, Phys. Rev. 83, 1085 (1951).
21. W. F. Cartwright, C. Richman, M. N. Whitehead, and H. A. Wilcox, The Production of Positive Pions by 341-Mev Protons on Protons, Phys. Rev. 91, 677 (1953).
22. W. H. Barkas, Threshold Energy for Meson Production, Phys. Rev. 75, 1109 (1949).
23. R. T. Birge, Calculation of Probable Errors, Phys. Rev. 40, 213 (1932).
24. A. J. Kirschbaum, Nuclear Absorption Cross Sections for High Energy Protons, Thesis, University of California Radiation Laboratory Report No. UCRL-1967, October, 1952.
25. L. L. Eyges, Multiple Scattering with Energy Loss, Phys. Rev. 74, 1535 (1948).
26. D. H. Stork, Total Positive Pion Cross Sections in Complex Nuclei, Thesis, University of California Radiation Laboratory Report No. UCRL-2288, July, 1953.
27. W. F. Cartwright, Production of π^+ -Mesons by 340-Mev Protons on Protons at 0° to the Beam, Thesis, University of California Radiation Laboratory Report No. UCRL-1278, April, 1951.
28. R. E. Marshak, Meson Physics, New York, McGraw-Hill Book Co., Inc., 1952.
29. E. M. Henley, π -Meson Production by Protons on Nuclei, Phys. Rev. 85, 204 (1952).
E. M. Henley and R. H. Huddleston, On the Production of π^+ Mesons in Carbon, Phys. Rev. 82, 754 (1951).
30. L. K. Neher, Meson Production by High-Energy Neutrons, Thesis, University of California Radiation Laboratory Report No. 2191, April, 1953.
31. W. Crandall, Phys. Rev. (in press).
32. E. L. Ginzton, W. R. Hewlett, J. H. Jasberg, and J. D. Noe, Distributed Amplification, Proc. I. R. E. 36, 956 (1948).

33. C. Wiegand, Distributed Coincidence Set, Rev. Sci. Instr. 21, 975 (1950).
34. R. S. White and G. Repp, private communication.
35. R. F. Post, Resolving Time of the Scintillation Counter, Nucleonics, June, 1951.
36. T. N. K. Godfrey, F. B. Harrison, J. W. Keuffel, Satellite Pulses from Photomultipliers, Phys. Rev. 84, 1248 (1951).